Research Article | Vol. 11, No. 12 / 1 December 2020 / Biomedical Optics Express 7376
Biomedical Optics EXPRESS

Nasal-temporal asymmetry in peripheral refraction with an aspheric myopia control contact lens

Durgasri Jaisankar,[1] Yongji Liu,[2] Pete Kollbaum,[3] Matt Jaskulski,[3] Paul Gifford,[4] Marwan Suheimat,[1] and David A. Atchison[1,*]

[1]*Centre for Vision and Eye Research, Queensland University of Technology, 60 Musk Avenue, Kelvin Grove, Queensland 4059, Australia*
[2]*Institute of Modern Optics, Nankai University, 38 Tongyan Road, Haihe Education Park, Tianjin 300350, China*
[3]*School of Optometry, Indiana University, Bloomington, IN 47405, USA*
[4]*School of Optometry and Vision Science, University of New South Wales, New South Wales, Australia*
[*]*d.atchison@qut.edu.au*

Abstract: A combination of human subject data and optical modelling was used to investigate unexpected nasal-temporal asymmetry in peripheral refraction with an aspheric myopia control lens. Peripheral refraction was measured with an auto-refractor and an aberrometer. Peripheral refraction with the lens was highly dependent upon instrument and method (e.g. pupil size and the number of aberration orders). A model that did not account for on-eye conformation did not mirror the clinical results, but a model assuming complete lens conformation to the anterior corneal topography accounted for the positive shift in clinically measured refraction at larger nasal field angles. The findings indicate that peripheral refraction of highly aspheric contact lenses is dependent on lens conformation and the method of measurement. These measurement methods must be reported, and care must be used in interpreting results.

1. Introduction

Numerous studies have investigated the potential use of multifocal contact lenses in controlling myopia progression [1–10]. Increasing negative refraction (or reducing positive refraction) in the peripheral visual field is thought to be a primary driver for this [11]. Interestingly, peripheral refraction with aspheric multifocal contact lenses, relative to unaided refraction, typically has more negative shift in the nasal visual field than in the temporal visual field. Specifically, peripheral refractions with both Proclear center-distance aspheric multifocal (CooperVision) contact lenses [1,12] and NaturalVue (Visioneering Technologies Incorporated) lenses [12] showed greater negative shift into the nasal than into the temporal visual field initially, but turning positive beyond 20° nasally (Fig. 1). The asymmetric peripheral refraction profile for the Proclear lens was less pronounced in one report [12] than in another [1].

There are possible reasons for the reported asymmetric peripheral refraction profile (Fig. 1). Sankaridurg *et al.* [2] wrote "A likely explanation for the asymmetry is that the lenses were systematically decentered from the visual axis, centering, as contact lenses usually do, on the geometric center of the cornea." Contact lens decentration and angles beyond 20° nasally may cause refraction to be taking place outside the optic zone of the contact lenses. The lower negative power of the lens carrier here may produce a positive shift in refraction. Pupil shape may be a factor, with the greater ellipticity nasally than temporally [13] meaning measurement beams are likely to pass quickly between optical and non-optical zones of the contact lens on the nasal side. Refraction results may be dependent on both the instruments and pupil diameters of the

#406101 https://doi.org/10.1364/BOE.406101
Journal © 2020 Received 21 Aug 2020; revised 9 Oct 2020; accepted 9 Nov 2020; published 1 Dec 2020

Biomedical Optics EXPRESS

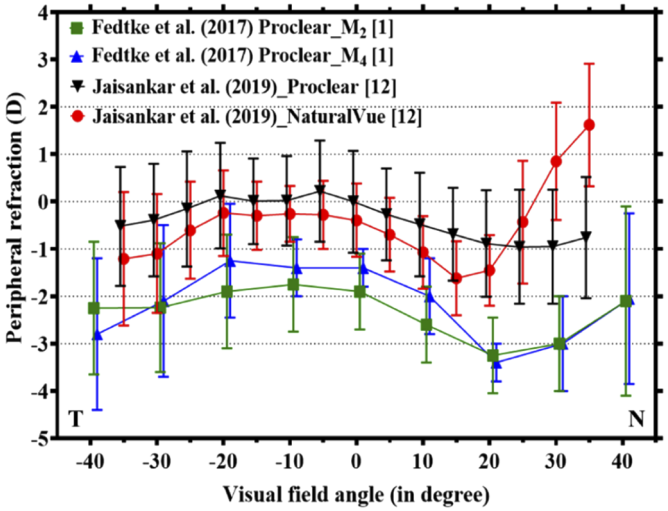

Fig. 1. Mean peripheral refraction results for Proclear center-distance multifocal contact lenses (+2.50 D add) with the BHVI-EyeMapper [1], and for Proclear center-distance (+2.50 D) and NaturalVue multifocal contact lenses with the Grand-Seiko WAM-5500 [12]. M_2 - calculated with 2^{nd}-order Zernike aberration terms and 3.0 mm pupils; M_4 - calculated with 2^{nd}- and 4^{th}-order Zernike aberration terms and 3.0 mm pupils; T - Temporal and N - Nasal. Error bars represent standard deviations.

subjects [14], and method used to quantify refraction. For example, the Grand-Seiko WAM 5500 auto-refractor/keratometer measures through an annulus of 1.5 mm inner and 2.3 mm outer diameters [15], and Hartmann Shack aberrometers capture data across the whole pupil from which the user can select the diameter of the region of analysis and the method to quantify the refraction [16] . We hypothesize these method-dependent factors affect what refractive state is reported and its interpretation on myopia control.

Accordingly, the purpose of this study was to systematically investigate factors leading to the reported temporal-nasal asymmetry in peripheral refraction found with NaturalVue lenses [12]. Specifically, aims were to understand effects of different instrument and analysis techniques on peripheral refraction and if these effects can be modeled successfully.

2. Methods

2.1. Participants

Table 1 provides relevant details of the 5 participants. Preliminary eye examinations screened for adverse effects of eye drops. One drop of 1% cyclopentolate was instilled 30 minutes prior to measurements in right eyes. In all measures the left eye was patched. The research followed the tenets of the Declaration of Helsinki and was approved by the University Human Research Ethics Committee, with informed consent obtained from participants.

2.2. Peripheral refraction

Peripheral refraction was obtained using two instruments; a Grand-Seiko WAM 5500 auto-refractor/keratometer (Grand-Seiko Co. Ltd., Tokyo, Japan) (henceforth termed “GS”) and a COAS-HD aberrometer (Wavefront Sciences Inc., Albuquerque, NM, USA) (henceforth termed “COAS”), both with and without wearing NaturalVue aspheric multifocal soft contact lenses (Etalfilcon A material, Visioneering Technologies Incorporated, Alpharetta, Georgia, USA). Lens powers were similar to those employed in the previous report describing the nasal-temporal

Biomedical Optics EXPRESS

Table 1. Participants' details

Participant no.	Age (years)	On-axis refraction (D)	Contact lens power (D)	Keratometry readings (D)
1	65	−1.25	−1.00	43.3 along 21.4°, 43.5 along 111.4°
2	42	−0.75	−1.00	42.6 along 132.9°, 42.9 along 42.9°
3	25	−0.25	+0.00	41.8 along 140.1°, 42.0 along 50.1°
4	21	−4.00	−4.00	43.9 along 54.6°, 44.5 along 144.6°
5	43	+0.37	+0.00	42.6 along 72.8°, 43.3 along 162.8°

peripheral refraction asymmetry [12]. Hashtag (#) fixation targets were positioned along the horizontal meridian out to ±35° in 5° intervals. Due to room space restraints, GS measurements were taken at 4 m while COAS-HD measures were taken at 3 m. With the GS the eye could fixate freely, but with the COAS-HD a periscopic system was mounted on the instrument head to allow monocular viewing of targets [17]. The periscopic system consisted of a relay system between the eye and the instrument which inverted the wavefront images upon capture, so these were inverted back prior to analysis. Prior to measurements, the instrument and the participant's right eye were aligned with the on-axis fixation target [12].

Five and two consecutive measurements were taken for the GS and COAS instruments, respectively, at each eccentricity. Only two measures were acquired with the COAS due to the longer acquisition and analysis time. The participant's head remained in the instruments between acquisition repetitions. Cycloplegic pupil diameters of all participants were all greater than 5 mm, and peripheral refractions were determined for both head and eye rotations. Consistent with previous studies [12,18–20], there was little difference between these methods, and so only head rotation results have been reported.

For the COAS, refractions were determined at pupil diameters of 2.3 mm (to match the outer diameter of the annulus sampled by the GS), 3.0 mm and 5.0 mm. The chin rest was attached to a rotational mount to ensure precise control of head rotation angles. Sphere S, cylinder C and axis θ of each GS measurement were converted to power vectors of mean sphere M, regular astigmatism J_{180} and oblique astigmatism J_{45} components using the equations [21]

$$M = S + \frac{C}{2} \tag{1}$$

$$J_{180} = \frac{-C\cos(2\theta)}{2} \tag{2}$$

$$J_{45} = \frac{-C\sin(2\theta)}{2} \tag{3}$$

For analysis of COAS measures, custom wavefront analysis software was written in MATLAB (R2013a, Mathworks, Natick, MA). This software horizontally stretched pupil data along their minor axes to form circular pupils, from which typical circular Zernike polynomial fitting approaches could be used [22]. The COAS software provides an image of the eye from which lengths of minor and major axes of an ellipse fit to the pupil shape can be determined for each eccentricity. The custom analysis software allows viewing the Hartmann-Shack spot centroid positions and altering them manually if not registered by the COAS firmware. As well as determining refractions, the software was used to investigate pupil and optic zone diameters (Fig. 2, Section 3.2).

Zernike coefficients up to 6th-order were fitted to the wavefront data for pupil diameters of 2.3 mm, 3 mm and 5 mm at 555 nm wavelength. Coefficients were converted to M, J_{180} and J_{45} components in two ways. First, including both lower and higher order (up to 6$^{\text{th}}$-order) Zernike

Biomedical Optics EXPRESS

terms gives [23]:

$$M = \frac{-[(2\sqrt{3}C_2^0 - 6\sqrt{5}C_4^0 + 12\sqrt{7}C_6^0)(1 + cos^2\phi) + (\sqrt{6}C_2^2 - 3\sqrt{10}C_4^2 + 6\sqrt{14}C_6^2)sin^2\phi)]}{r^2cos^2\phi} \quad (4)$$

$$J_{180} = \frac{-[(2\sqrt{3}C_2^0 - 6\sqrt{5}C_4^0 + 12\sqrt{7}C_6^0)sin^2\phi + (\sqrt{6}C_2^2 - 3\sqrt{10}C_4^2 + 6\sqrt{14}C_6^2)(1 + cos^2\phi)]}{r^2cos^2\phi} \quad (5)$$

$$J_{45} = \frac{-[(2\sqrt{6}C_2^{-2} - 6\sqrt{10}C_4^{-2} + 12\sqrt{14}C_6^{-2})cos\phi]}{r^2cos^2\phi} \quad (6)$$

where r is pupil major semi-diameter and ϕ is visual field angle. The second way was to use only 2nd-order co-efficients C_2^0, C_2^2 and C_2^{-2} in the equations. These equations assume the off-axis pupil as acquired was elliptical in shape with dimension $r\cos\phi$ along its minor axis.

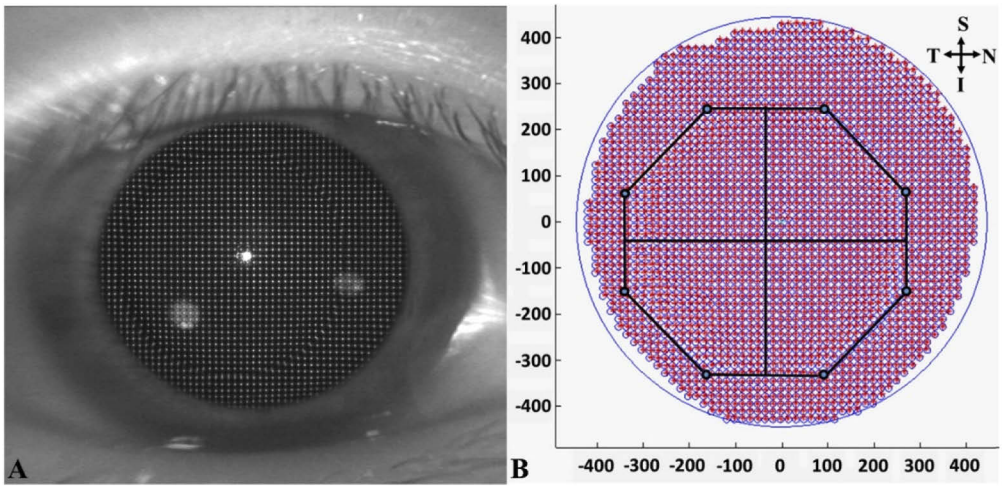

Fig. 2. Determination of optic zone diameter with 8 mm measuring zone (100 normalized pixels = 1 mm). (A) Composite image of iris image and retinal image taken in COAS. (B) The centroid image reproduced by the wavefront analysis software. The sudden off-set of the aberrated centroids (pink points) from the reference centroids (blue circles) marks the edge of the optical zone of the contact lens. Eight points were marked at the edges of the optic zone. Points were connected to form an octagon. The vertical and horizontal diameters of the octagon were measured. Co-ordinates with respect to eye: I- Inferior, S- Superior, N- Nasal, T- Temporal.

2.3. *Off-eye power of NaturalVue lenses*

Off-eye power profiles of NaturalVue lenses were determined to approximately ±3.8 mm distance from center using custom software and zonally reconstructed wavefronts obtained from a single pass aberrometer (ClearWave, Lumetrics; Rochester, NY). The lens was within a saline filled wet cell and corrected for this using lens base radius, refractive index and thickness. The instrument uses a collimated visible light source with wavelength of 540 nm and a 101 × 101 lenslet array with a 10.4 × 10.4 mm field of view to provide a spatial resolution of 104 microns [24]. There were radially symmetrical power changes from center to the edge of the lenses across horizontal profile, vertical profile and radial average (Fig. 3). Lens powers increased by 2.50 D to 3.00 D at ±3 mm from centers, followed by sharp drops.

Biomedical Optics EXPRESS

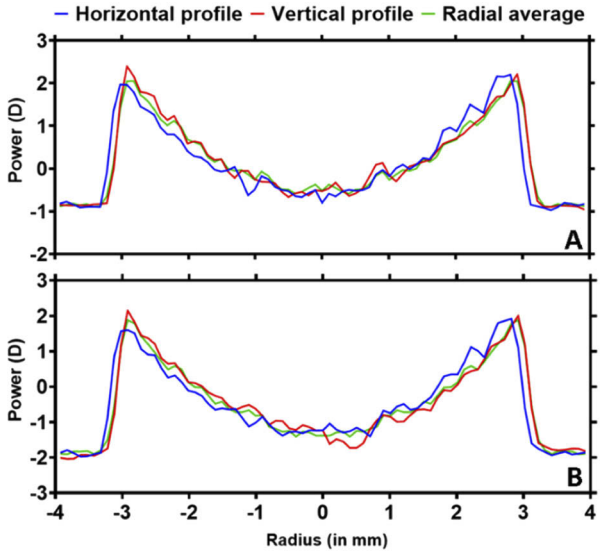

Fig. 3. Power profiles, with a ClearWave aberrometer, of NaturalVue contact lenses from same manufacturing batch as used in the study with distance zone powers (A) +0.00 D and (B) −1.00 D.

2.4. Biometry measurements of anterior eye and on-eye contact lenses

Using a Pentacam instrument (Oculus, Hesse, Germany), mean anterior corneal radius of curvature, mean posterior corneal radius of curvature, corneal center thickness, and anterior chamber depth were determined for each participant. Assuming refractive indices for cornea and anterior chamber depth of 1.376 and 1.336, anterior corneal surface position relative to entrance pupil was calculated.

An E300 videokeratoscope (Medmont Pty Ltd, Melbourne, Australia) was used to capture topography without and with NaturalVue contact lenses on the eye. The without-lens condition means that the anterior cornea was being measured and with-lens means that anterior surface of a lens was being measured. Four consecutive measurements were taken without-lens and approximately ten consecutive measurements were taken with-lens. As it was difficult to take good measurements with contact lenses in place, several measurements were obtained in order to ensure an equal number of comparable good images to that of without-lens. Images were processed using Medmont Studio 6 software, and corneal topography data for each image was exported using both the program's standard export function, to extract pupil coordinates relative to the videokeratoscope measurement axis, and its raw export function to extract the maximum available corneal topography measurement data points.

2.5. Contact lens decentration on-eye

Ocular images during lens wear were taken from the direction of gaze with a smartphone camera (iPhone 8 plus, Apple Inc., Sydney, NSW, Australia) at 0°, and also at ±35° eccentricities which confirmed that decentration remained consistent at the extreme visual angles with head rotation. Contact lens decentration was calculated using a calibrated, repeatable image processing technique (Adobe Photoshop CS5 and Microsoft Office PowerPoint 2016) [12].

Biomedical Optics EXPRESS

2.6. Eye model simulations

Eye model simulations were carried out for participants 1 and 2 using two models representing the extreme situations where the lens does not conform to the corneal surface and where the lens completely conforms. In model 1, the anterior contact lens surface was determined using an off-eye aberrometer where the lens was positioned in a wet cell, maintaining its inherent curvature (Section 2.3). In model 2, the anterior contact lens surface was determined using on-eye topographical measurements of the cornea wearing a contact lens (Section 2.5). These two models represent the extreme cases in which the lens may fail to wrap on the eye and wrap completely to the eye. Results may agree with either or be somewhere between the two outcomes. Common features of the models are described here, while more model specific details are described in Sections 2.6.1 and 2.6.2.

Out-of-the eye raytracing (Fig. 4) was implemented in Zemax (Radiant Zemax, Kirkland, Washington, USA) in which a target was located at infinity. This was done for 2.3 mm, 3.0 mm and 5.0 mm pupils. A series of simulated phase plates, with different wavefront aberrations for each visual field angle from (−)35° temporal to (+) 35° nasal, represented peripheral wavefront aberrations of an eye without a contact lens. Each phase plate was located at the entrance pupil of the eye.

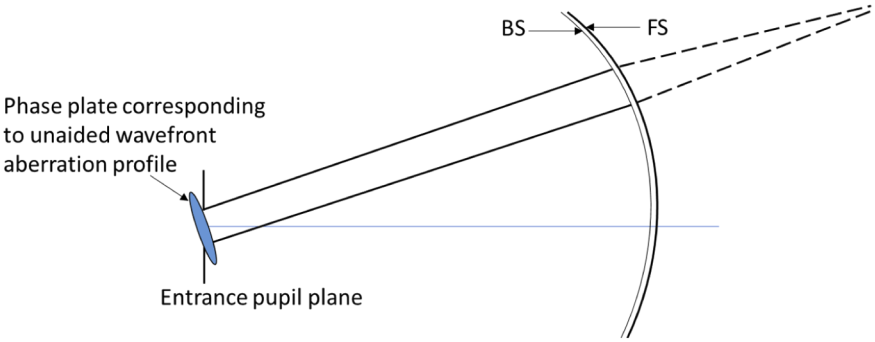

Fig. 4. Out-of-the eye raytracing to model peripheral refraction. For Model 1, FS is the modeled front surface of the in-vitro contact lens and BS is the matching spherical back surface. For Model 2, FS is the Zernike surface polynomial of the front surface of the on-the-eye contact lens and BS is the Zernike surface polynomial of the back surface (considered to match the anterior cornea).

Lens central thicknesses and refractive indices in the models were slightly different (0.059 mm and 1.400 in model 1, 0.08 mm and 1.402 in model 2) but these differences had minimal effect on results. Decentrations and tilts of contact lens surfaces relative to the line-of-sight were determined using data from the Pentacam instrument (Section 2.4) and the following equations [25]. Decentrations and tilts were simulated as "coordinate breaks" in Zemax (Fig. 5):

$$x = \frac{TCPC_x}{WD + EP}; y = \frac{TCPC_y}{WD + EP} \tag{7}$$

$$\theta_x = \tan^{-1}\left(\frac{x}{WD}\right); \theta_y = \tan^{-1}\left(\frac{y}{WD}\right) \tag{8}$$

Here EP is entrance pupil distance inside the eye (and becomes the stop for raytracing), θ_x and θ_y are horizontal and vertical angles between the line-of-sight and the videokeratometric axis, $TCPC_x$ and $TCPC_y$ are horizontal and vertical decentration components of the videokeratometric axis from the pupil center as obtained from topography images with a E300 videokeratoscope (Medmont Pty Ltd, Melbourne, Australia), and x and y are horizontal and vertical decentration

Biomedical Optics EXPRESS

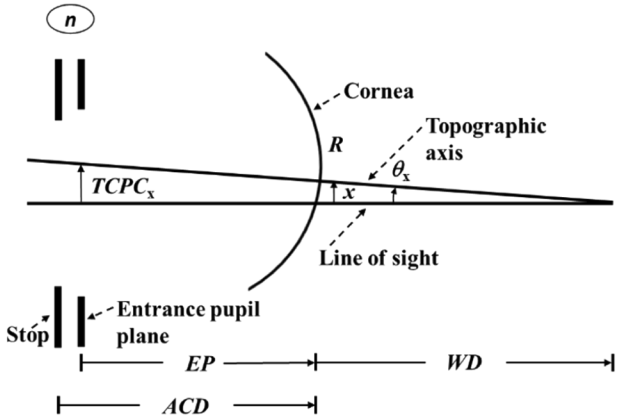

Fig. 5. Calculation of corneal decentration and tilt in horizontal meridian. See text for details.

components of the anterior corneal vertex from the line-of-sight. *WD* is the distance from the cornea to the instrument target plane and is 60.047 mm. For model 1, conversions from (TPC_x, TPC_y) to (x, y) were not necessary as contact lens displacement (x, y) was measured according to Section 2.5. θ_x and θ_y were still determined from Eq. (8).

Wavefront aberration coefficients were determined at the exit pupil of the system (image of entrance pupil in contact lenses), which given the low lens powers was close to the entrance pupil. M, J_{180} and J_{45} refraction components were calculated according to Eqs. (4)–(6).

2.6.1. Model 1 assuming no lens conformation to the cornea

The radial power profiles of the NaturalVue lenses (Fig. 3) were further smoothed in OriginPro 2018C (OriginLab, Wellesley Hills, MA, USA). Contact lens front surfaces were modeled using the Binary Optic 4 surface type in the optical design program Zemax to match these power profiles. This surface type supports a variety of concentric optical zones of different powers with independent radial diameters, conic and polynomial aspheric coefficients. The outer diameter was 8.0 mm, but the measured power profile was within a diameter of 7.45 mm.

Each front surface was modelled by the following steps:

i) The initial central thickness was 0.07 mm, refractive index 1.400 and back surface radius of curvature to be 8.3 mm, the same as the nominally manufacturer specified base curve of the NaturalVue multifocal contact lens. The back surface was assumed to be spherical.

ii) Because the power profile of NaturalVue contact lenses changes significantly (Fig. 6), the anterior surface was segmented into four zones. For the −1.00 D lens, these had semi-diameters of 1.5 mm, 3.0 mm, 3.3 mm and 4.0 mm. The sag z_j (r) at a radial distance r in the j^{th} zone was given by the equation

$$z_j(r) = \frac{c_j r^2}{1 + \sqrt{1 - (1 + k_j)c_j^2 r^2}} + \sum_{i=1}^{N_a} \alpha_{ji} p^{2i} + z_0 \tag{9}$$

where j has values from 1 to 4, c_j is the curvature of the j^{th} zone, k_j is the corresponding conic constant for the zone, α_{ji} terms are aspheric coefficients for the zone, N_a is the number of figuring terms for each zone (chosen as four), p is the normalized coordinate of the zone given by r/A_j where A_j is the semi-diameter of the zone, and z_0 is chosen to make

Biomedical Optics EXPRESS

the surface continuous across the boundary between the current and prior zone at radial coordinate A_{j-1}.

iii) The radius of curvature of the front surface within the first (inner) zone, its aspherical coefficient and the central thickness were set as variables. Operands controlled the effective focal length, the central thickness, and the edge thickness. The zone was optimised through raytracing so that the powers profile matched that of the smoothed values.

iv) For the second zone, the central thickness obtained in the previous step was retained (0.059 mm). The radius of curvature of the zone and the aspherical coefficients were set to be variables. The third and fourth zones parameters were determined similarly.

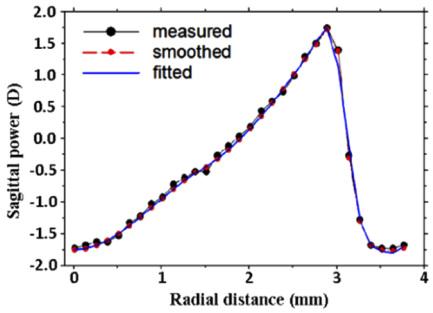

Fig. 6. Sagittal power of −1.00 D NaturalVue lens as a function of radial distance from lens center.

The simulated power profile of a −1 D lens, that used for participants 1 and 2, is shown in Fig. 6; this is an excellent fit to the smoothed values.

2.6.2. Model 2 assuming complete lens conformation to the cornea

A custom written MATLAB program was used to extract corneal elevation data (Section 2.4) from each Medmont E300 raw data export file. This was done for a representative image for each participant/lens condition. The software fitted Zernike surface coefficients up to the 12th

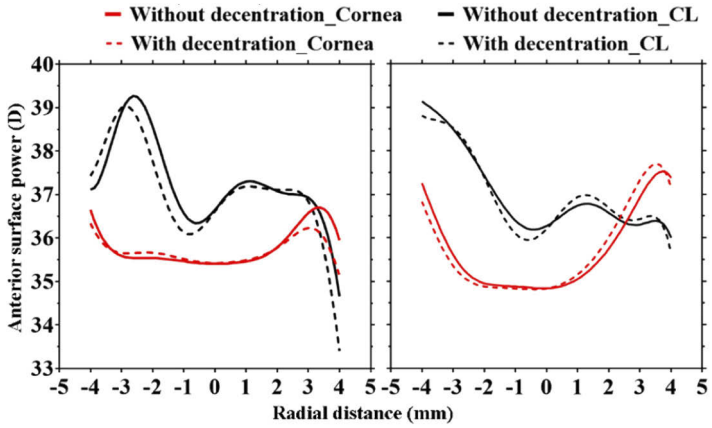

Fig. 7. Horizontal meridian refractive power profiles of centered and decentered anterior surfaces for participant 1 (left) and participant 2 (right) of corneas and of NaturalVue contact lenses. Positive radial distance represents the nasal side.

Biomedical Optics EXPRESS

order across a 10.8 mm diameter, and wrote the Zernike coefficient values to an electronic file in Zemax optical design data file format. Zernike surface coefficients were used to promote a smooth optical corneal surface profile within Zemax that is not possible by directly importing raw corneal surface sag heights.

A second custom *MATLAB* program read the pupil (X, Y) coordinates relative to the videokeratoscope axis from each corneal topography Medmont standard export file to allow calculation of corneal surface decentration and tilt relative to the line-of-sight. Figure 7 shows anterior surface powers of corneas and NaturalVue lenses for participants 1 (left) and 2 (right), without and with decentration (and tilt).

3. Results

3.1. Comparison between peripheral refractions

3.1.1. Measured GS vs. COAS including higher order terms up to 6th-order

Without-lens peripheral mean refraction values (M) showed little differences between GS and COAS in all participants except for participant 1 (Fig. 8, row 2, column 1) for whom the COAS 2.3 mm and COAS 3 mm diameter data were noticeably more negative on-axis and at ±5° than the GS and COAS 5 mm results. Maximum mean differences (COAS – GS) without-lens were −0.9 D at +30° (2.3 mm), −0.7 D at +35° (3 mm) and −1.0 D at +35° (5 mm).

With-lens peripheral mean refraction between GS and COAS were irregular for most participants (Fig. 8, column 2) and these differences beyond 25° were greater in the nasal field than in the temporal field. Three participants showed slightly more negative peripheral refraction with the GS compared with the COAS for most temporal field angles, but participants 1 and 2 showed the opposite. Most participants showed slightly less negative peripheral refraction with the GS than the COAS for most nasal field angles. As expected, due to the large power change across the lens surface, the GS result was closer to the COAS 2.3 mm and 3 mm diameter results than to the COAS 5 mm results in both fields. A positive shift in refraction at high nasal field angles occurred for all participants with both instruments. The angles at which the shift started were similar between the GS and COAS 5 mm results for most participants, whereas for the COAS 2.3 mm and 3 mm results the shift started 5 to 10° beyond that of the GS. The maximum mean differences (COAS – GS) were at +30°: −2.6 D (2.3 mm), −3.0 D (3 mm) and −2.0 D (5 mm).

As the J_{180} component of astigmatism varied much more than the J_{45} component across the horizontal field, only results of the former are shown (Fig. 9). Without-lens results were similar between GS and COAS in all participants, showing the characteristic inverted parabola shape (column 1). With-lens, GS results show dramatic shifts in the positive direction beyond 15° nasal, but for all COAS pupil sizes the positive shift did not occur until approximately +25°.

3.1.2. Measured GS vs. COAS refraction with only 2nd-order terms

For the without-lens condition the COAS peripheral mean refraction results were similar regardless of whether only 2nd-order or higher-order terms were included (compare Figs. 8 and 10). GS refractions were closer to those of the COAS 2.3 mm and COAS 3 mm results than they were to those of the COAS 5 mm for most participants, due to the larger annular data encompassing more of the naturally occurring radially symmetric power change of the eye. The mean differences in M between GS and COAS were less than or equal to 1.0 D. The maximum differences (Fig. 10, row 1 column 1) were −0.9 D at 35° (2.3 mm), −0.9 D (3 mm) at 35° and −1.0 D (5 mm) at 25°.

Relative mean peripheral refractions for the with-lens condition with GS were closer to 2nd-order only COAS results than they were to COAS results which also included terms up to the 6th-order (Figs. 8 and 10, column 2). The positive shift at high nasal field angles occurred for all participants both with the GS and COAS. Generally, GS refractions were closer to those of the COAS 2.3 mm and 3 mm than they were to the COAS 5 mm results. The maximum mean

Biomedical Optics EXPRESS

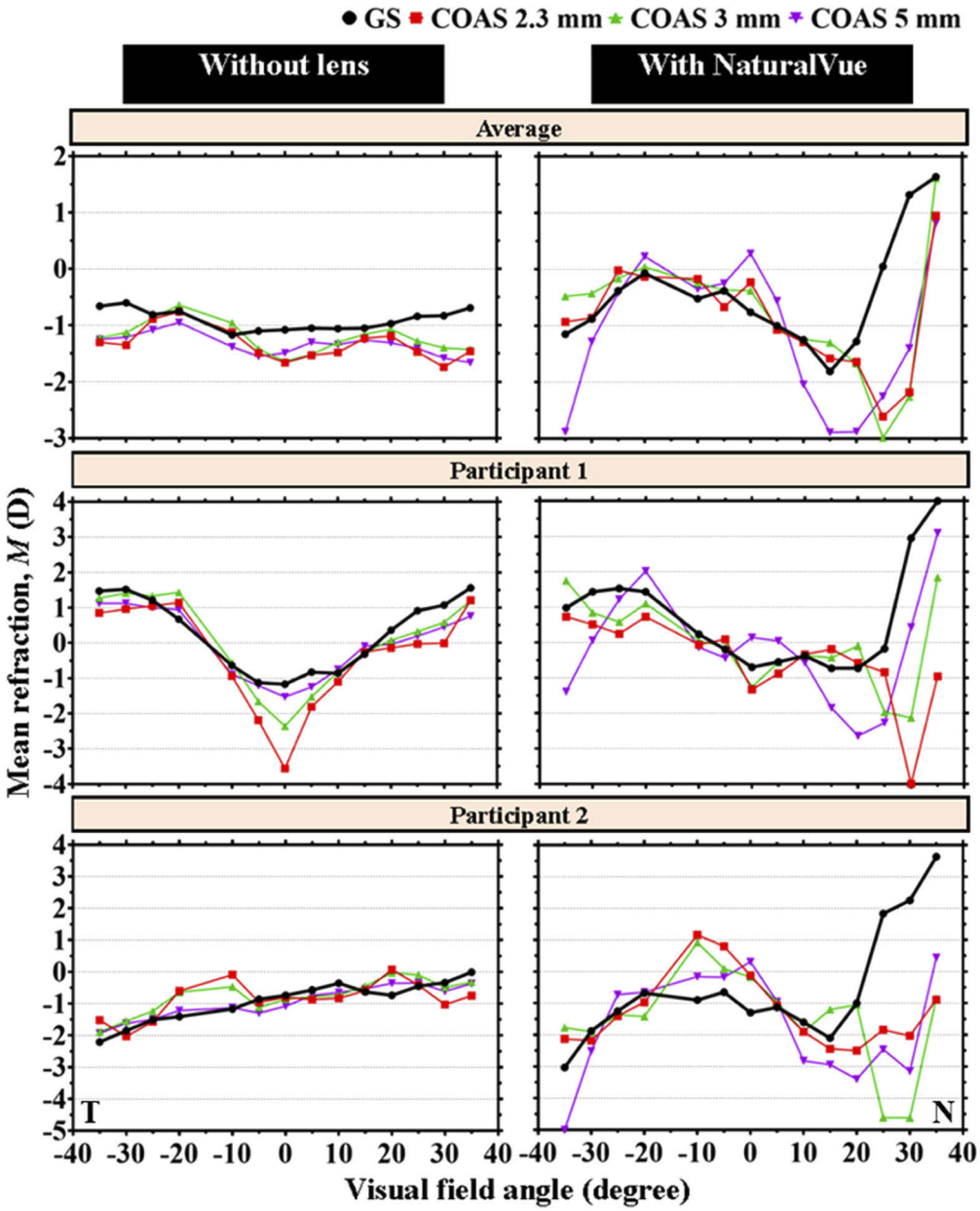

Fig. 8. Mean refraction (M) as a function of visual field angle without-lens and with the NaturalVue lens in GS and in COAS with terms up to the 6th-order. Results shown are the means of all participants (top row), participant 1 (middle row) and participant 2 (bottom row). Note differences in vertical scales. N - positive angles, T - negative angles.

Biomedical Optics EXPRESS

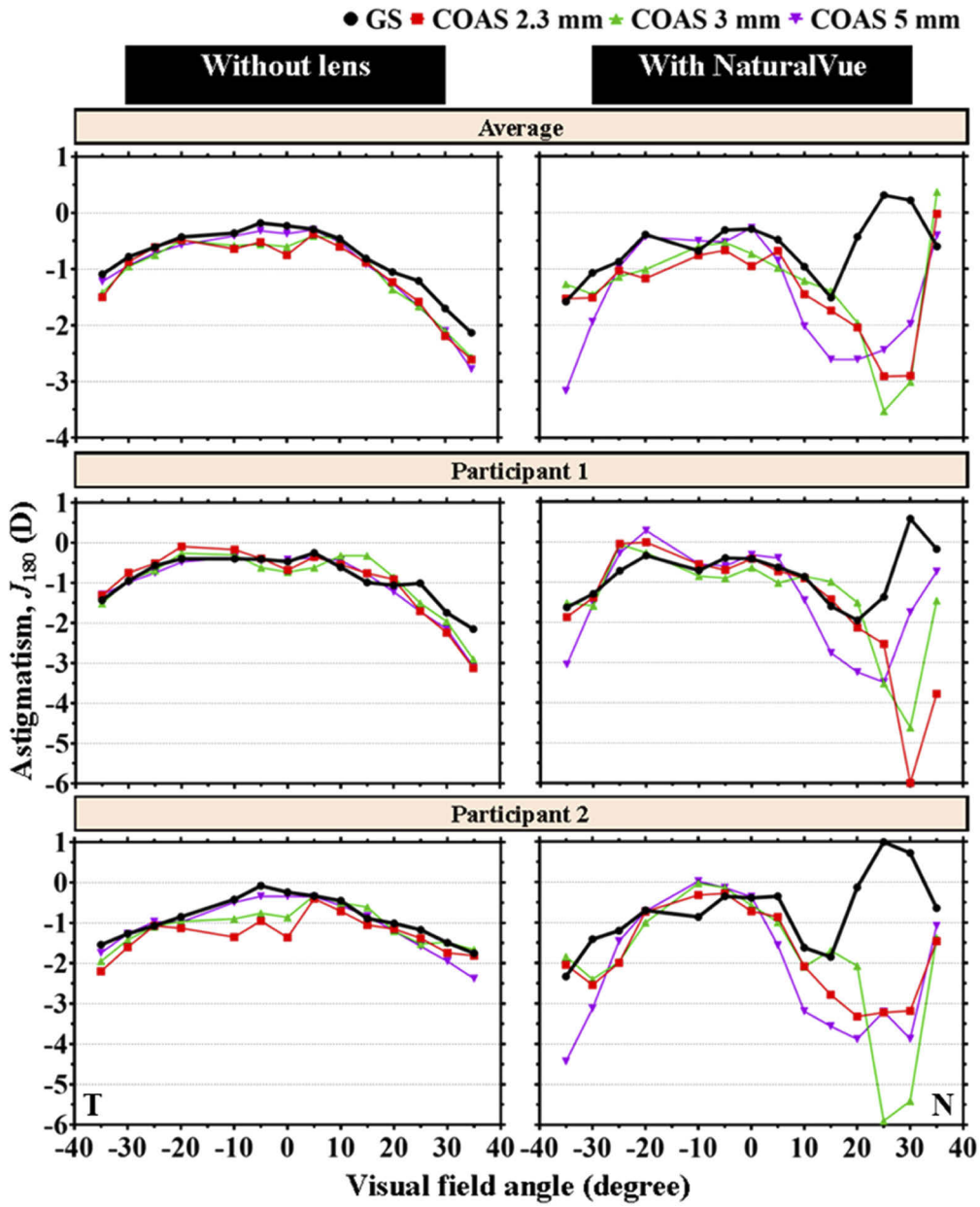

Fig. 9. J_{180} component of astigmatism as a function of visual field angle without-lens and with the NaturalVue lens in GS and in COAS with terms up to the 6th-order. The results shown are the means of all participants (top row), participant 1 (middle row) and participant 2 (bottom row). Note the differences in vertical scales.

Biomedical Optics EXPRESS

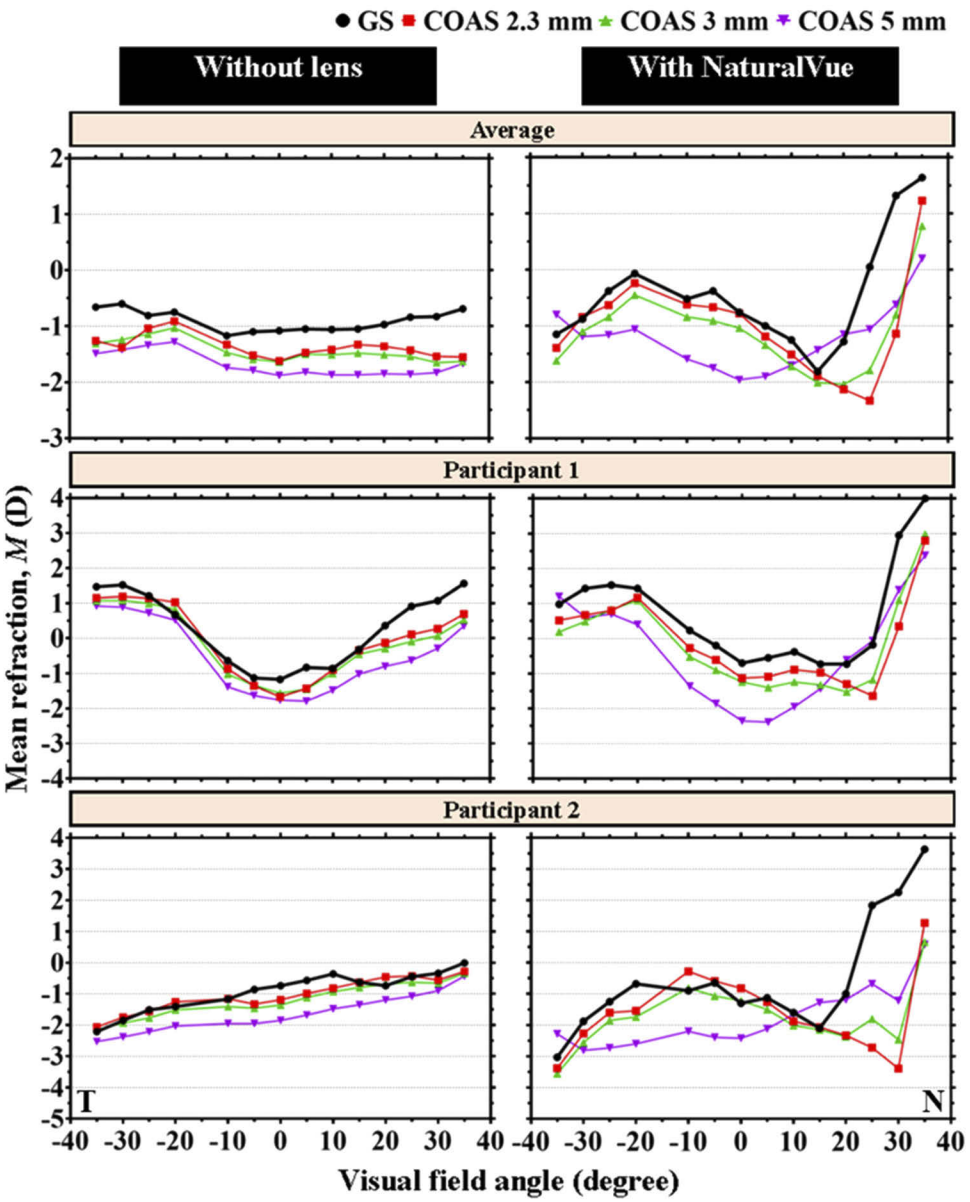

Fig. 10. Mean refraction (M) as a function of visual field angle without-lens and with the NaturalVue in GS and in COAS with only the 2nd-order terms. The results shown are the means of all participants (top row), participant 1 (middle row) and participant 2 (bottom row). The vertical scales are the same as for Fig. 8.

Biomedical Optics EXPRESS

differences (COAS – GS) were −1.8 D at +25° (2.3 mm), −1.3 D at +30° (3 mm) and −0.9 D at +30° (5 mm).

The J_{180} variations in the nasal visual field were not as marked for 2nd-order only COAS results as for COAS results including terms up to the 6th-order (Figs. 9 and 11, column 2). For the former, positive shift did not occur for 5 mm pupils.

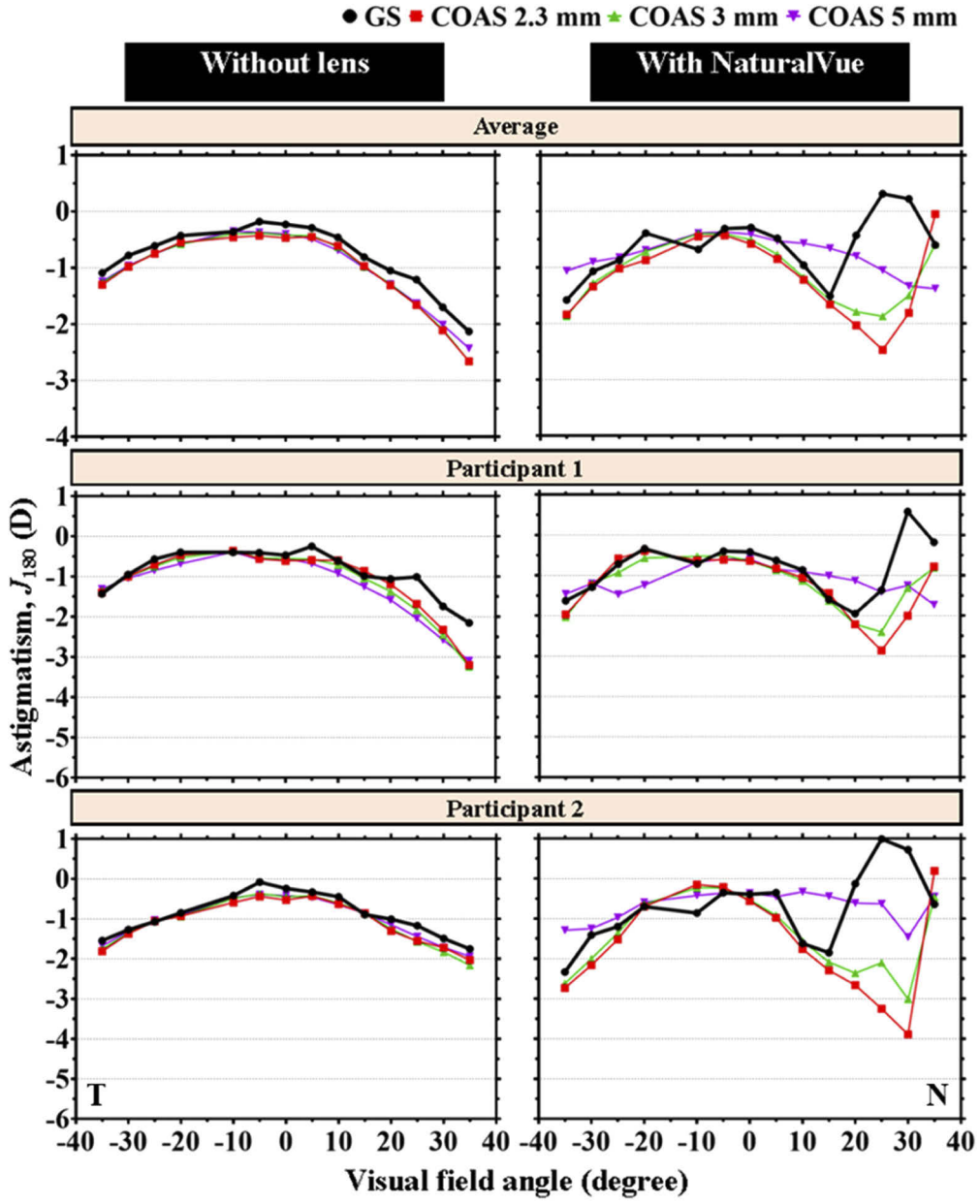

Fig. 11. J_{180} component of astigmatism as a function of visual field angle without-lens and with the NaturalVue in GS and in COAS with only the 2nd-order terms. The results shown are the means of all participants (top row), participant 1 (middle row) and participant 2 (bottom row). The vertical scales are the same as for Fig. 9.

Biomedical Optics EXPRESS

3.1.3. Summary

GS mean refractions were generally closer to the smaller analysis diameter results of the COAS (2.3 and 3.0 mm) than to the 5 mm results. GS refractions were also closer to the COAS when using only 2^{nd}-order terms than they were to COAS including 2^{nd}–6^{th} order terms. As expected, larger diameter analyses and higher order refraction measures were affected by the rapid power changes across the lens surface.

3.2. Pupil diameter without a lens and pupil diameter corresponding to the optic zone with NaturalVue lenses

Figure 12 shows the horizontal diameters of pupils without-lens and the horizontal diameter of pupils corresponding to the optic zone with-lenses for each participant. Diameters decreased into both temporal and nasal fields, but as expected [13], more rapidly for the latter. The pupil diameters with-lenses were similar to without-lens and are not shown. The vertical pupil and optic zone diameters did not alter with visual field angles and are not shown.

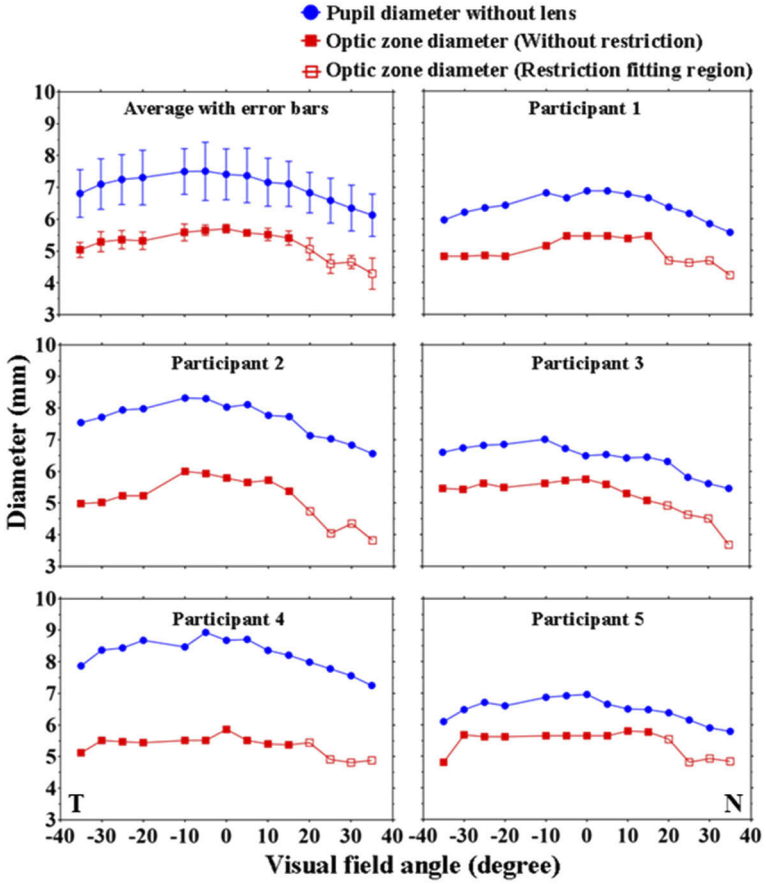

Fig. 12. Horizontal diameter of pupil without-lens and that corresponding to the optic zone with-lens as a function of visual field. Error bars are 95% CIs of means. The optic zone diameter was based on restriction fitting region beyond 15° nasal visual field.

Biomedical Optics EXPRESS

3.3. Simulations

Figures 13 and 14 show the measured and modelled peripheral mean refraction results of participants 1 and 2, respectively. Using 2nd order fits, for both participants the predictions of models 1 and 2 were similar from −35° to −10° and both aligned reasonably with GS and COAS data. Beyond −10° the predictions of the models began to differ considerably. Model 1 had more positive values than model 2 between −10° and +10°. Importantly, beyond +10° model 2 picked up the positive (hyperopic) shift in measurements whereas model 1 generally did not. Model 2 gave similar predictions for GS and COAS for participant 1 and better predictions for GS than COAS for participant 2. Findings for the 6th order fits were similar to those for second order fits, except agreement of modeling with GS and COAS results was poorer in the −35° to −10° range.

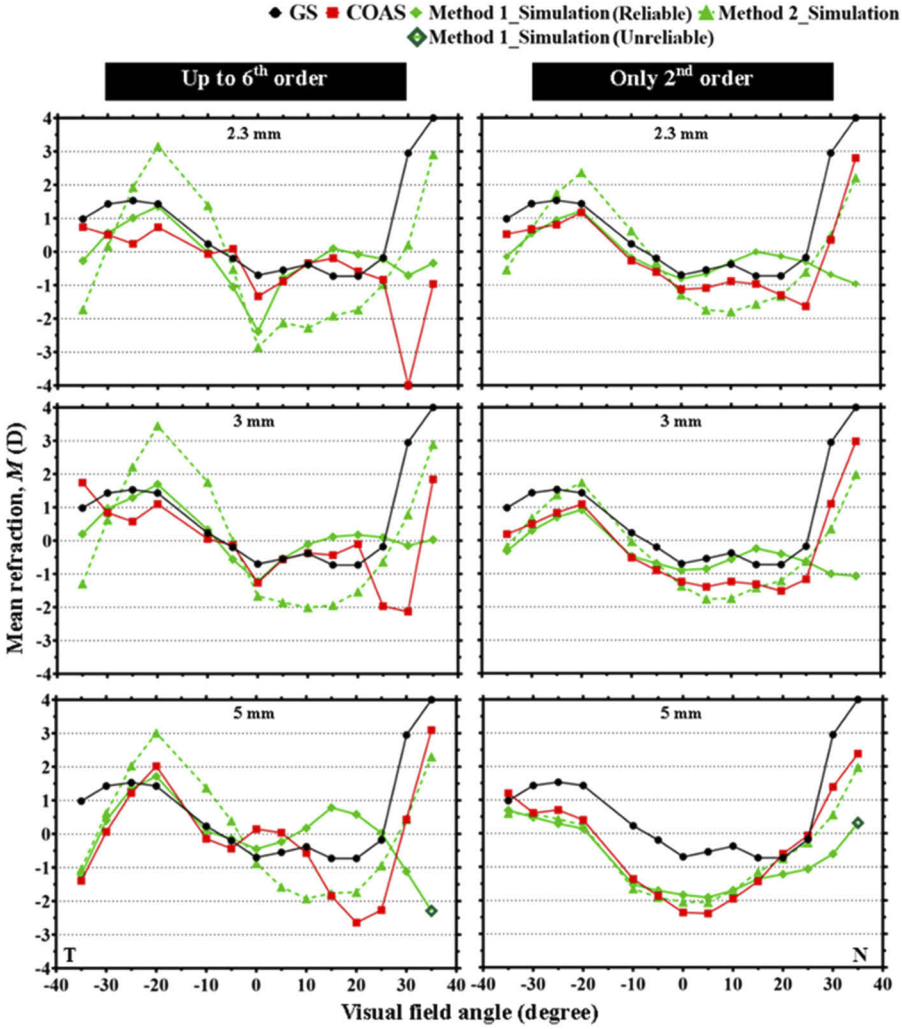

Fig. 13. Mean refraction (M) as a function of visual field angle with NaturalVue lens for participant 1. Left column: GS, 2nd–6th-order for COAS and COAS simulation. Right column: GS, 2nd-order for COAS and COAS simulation. Model 1 simulation for 5 mm pupil was unreliable beyond 30° in the nasal visual field; contact lens decentration for simulation was (−0.07 mm, −0.52 mm).

Biomedical Optics EXPRESS

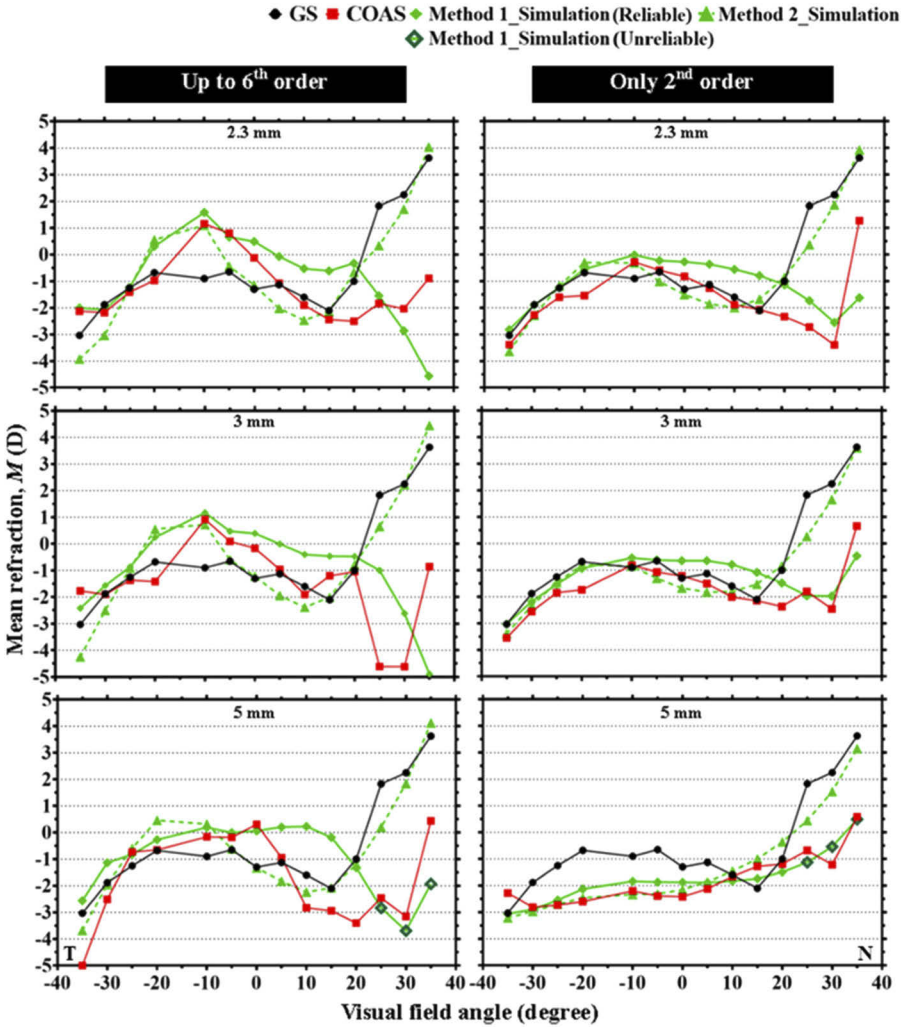

Fig. 14. Mean refraction (M) as a function of visual field angle with NaturalVue lens for participant 2. Left column: GS, 2^{nd}–6^{th}-order for COAS and COAS simulation. Right column: GS, 2^{nd}-order for COAS and COAS simulation. Model 1 simulation for 5 mm pupil was unreliable beyond 20° in the nasal visual field; contact lens decentration for simulation was (−0.44 mm, 0.13 mm).

Biomedical Optics EXPRESS

4. Discussion

This study aimed to investigate the nasal-temporal asymmetry in GS measured peripheral refraction with highly aspheric multifocal NaturalVue myopia control lenses and provide information on how peripheral refraction with these lenses differed between commonly utilized clinically techniques.

Without lenses, refractions were similar between the instruments for most visual field angles, thus supporting previous studies [26–28]. Similar to the previous study [12], the NaturalVue lens showed dramatic positive shifts of mean refraction in the nasal field for both GS (beyond +15° to +20°) and COAS (beyond +20° to +25°).

The peripheral refraction patterns with NaturalVue were considerably different between GS and COAS instruments. Those for COAS were affected by analysis size and order of fit, with closer alignment to the GS results for smaller pupil sizes and fewer orders. Bakaraju *et al.* [27] also found considerable differences in peripheral refraction with multifocal soft contact lenses between a Shin-Nippon NVision K5001 autorefractor (similar to GS) and the COAS-HD with 3 mm pupils.

As with measured data, there were significant differences in the predictions of the individualized eye models. Neither model showed complete agreement with either the GS or COAS instruments, but the on-eye model 2 which assumed lens conformation to the cornea did an excellent job of predicting the temporal-nasal asymmetry; unlike model 1 it shows the positive shift in refraction at the larger nasal field angles (Figs. 13 and 14). This indicates deformation of the contact lens on the eye, perhaps warping on the nasal side to give negative shift in power relative to that of the anterior cornea (Fig. 7).

Differences in modelling predictions were affected by model inputs. For in-vitro model 1 we used the wave aberration of the contact lens when it was inside a wet-cell filled with saline. We applied a conversion of the measurement to in-air equivalent, but there may have been off-eye flexure effects which can occur for thin soft lenses like the NaturalVue [24]. Model 1 also assumed the back surface to be a spherical surface. Alternatively, model 2 assumes the back surface to match the anterior cornea, i.e. the degree of conformation limits model predictions. There is also the issue as to how well Zernike polynomials modelled surfaces, though we are confident that by calculating to the 12^{th} order Zernike corneal surface representation will match or exceed the measurement accuracy of the E300 keratometer [29].

While the asymmetry in the lens on the eye seems to be the main factor contributing to the temporal-nasal asymmetry in peripheral refraction, there are two other factors. Firstly, if a lens is decentered temporally smaller angles are required to pass beyond the optic zone in the nasal field. Lenses in this current study were decentered temporally, considerably more for participant 2 than participant 1 (−0.44 mm and −0.07 mm, respectively). Secondly, pupil size narrows horizontally more quickly in the nasal than in the temporal visual field (Fig. 12), such that the diameter at −35° is similar to or even greater than that at +20° for most participants. The axis of the pupil aligns with a ~6° temporal field [13] which should also add to the effect of passing through the ~6 mm diameter optic zone more quickly with a small pupil than with a large pupil, and aid the rapid positive shifts seen in the nasal field. The modelling includes the first, but not the second of these factors. However, our calculations, both for general aberration and modelling assuming that the pupil closes down horizontally as the cosine of the field angle, seem to be reasonable for the nasal field (Fig. 7).

Related to the second point is that many peripheral field aberration analyses with aberrometers use circular pupils rather than elliptical pupils [30]. While this may affect aberration analyses under some circumstances, some checking with one participant's data indicated that this did not have a big influence on refractions.

This work highlights differences in refraction interpretation based on the pupil size analysed. Of course, in the real-world, pupil size will vary with environment, task, age, and many other factors [31]. Although GS measures are acquired at a fixed diameter, no standard for COAS

Biomedical Optics EXPRESS

measures of refraction exits. Some have suggested 3 or 4 mm [32] as the diameter which optimally correlates with subjective refractions, but further work is needed in this area. The current study, however, importantly highlights that different interpretations can be made depending on pupil size utilized to obtain the reported refraction.

To conclude, peripheral refraction with highly aspheric lenses, like the NaturalVue aspheric multifocal contact lens, depend critically on the instrument with which it is measured, and for aberrometers, the analysis diameter and number of aberration orders. Anterior lens surface modelling on eye indicates that lens warping in-situ accounts for the positive shift in refraction that was measured at larger nasal field angles. The refraction measures derived from COAS measurements in the current study may not be optimized, and further work can explore alignment of measured and modeled results with those predicted by image quality metrics [6,33]. The current work also shows that, as previously identified [34], on-eye lens flexure effects cannot be negated. This current work indirectly highlights that small errors in lens conformation to the cornea can lead to large differences in the dioptric power provided to the retina.

It is essential that manufacturers of myopia control lenses aim to provide lenses with the optimal conformation to the cornea and optimal pupil centration. It is also essential that clinicians fitting these myopia control lenses understand the importance that small dislocations and lens flexure effects may have on the patient's clinical outcomes. Ideally to enhance myopia control outcomes, improved metrology will develop which aids the clinician to better quantify these effects accurately and efficiently in a clinical practice.

Acknowledgements

Durgasri Jaisankar is a recipient of Queensland University of Technology Postgraduate Research Award.

Disclosures

The authors declare no conflicts of interest.

References

1. C. Fedtke, K. Ehrmann, V. Thomas, and R. C. Bakaraju, "Peripheral refraction and aberration profiles with multifocal lenses," Optom. Vis. Sci. **94**(9), 876–885 (2017).
2. P. Sankaridurg, B. Holden, E. Smith, T. Naduvilath, X. Chen, P. L. de la Jara, A. Martinez, J. Kwan, A. Ho, and K. Frick, "Decrease in rate of myopia progression with a contact lens designed to reduce relative peripheral hyperopia: one-year results," Invest. Ophthalmol. Visual Sci. **52**(13), 9362–9367 (2011).
3. N. S. Anstice and J. R. Phillips, "Effect of dual-focus soft contact lens wear on axial myopia progression in children," Ophthalmology **118**(6), 1152–1161 (2011).
4. X. Cheng, J. Xu, K. Chehab, J. Exford, and N. Brennan, "Soft contact lenses with positive spherical aberration for myopia control," Optom. Vis. Sci. **93**(4), 353–366 (2016).
5. D. Lopes-Ferreira, C. Ribeiro, R. Maia, N. García-Porta, A. Queirós, C. Villa-Collar, and J. M. González-Méijome, "Peripheral myopization using a dominant design multifocal contact lens," J. Optom. **4**(1), 14–21 (2011).
6. R. Rosén, B. Jaeken, A. Lindskoog Petterson, P. Artal, P. Unsbo, and L. Lundström, "Evaluating the peripheral optical effect of multifocal contact lenses," Ophthalmic Physiol. Opt. **32**(6), 527–534 (2012).
7. D. Lopes-Ferreira, C. Ribeiro, H. Neves, M. Faria-Ribeiro, A. Queirós, C. Villa-Collar, J. Jorge, and J. M. González-Méijome, "Peripheral refraction with dominant design multifocal contact lenses in young myopes," J. Optom. **6**(2), 85–94 (2013).
8. A. Queirós, D. Lopes-Ferreira, and J. M. González-Méijome, "Astigmatic peripheral defocus with different contact lenses: review and meta-analysis," Curr. Eye Res. **41**(8), 1005–1015 (2016).
9. A. Ticak and J. J. Walline, "Peripheral optics with bifocal soft and corneal reshaping contact lenses," Optom. Vis. Sci. **90**(1), 3–8 (2013).
10. P. Kang, Y. Fan, K. Oh, K. Trac, F. Zhang, and H. A. Swarbrick, "The effect of multifocal soft contact lenses on peripheral refraction," Optom. Vis. Sci. **90**(7), 658–666 (2013).
11. E. L. Smith III, L.-F. Hung, and J. Huang, "Relative peripheral hyperopic defocus alters central refractive development in infant monkeys," Vision Res. **49**(19), 2386–2392 (2009).
12. D. Jaisankar, A. Leube, K. L. Gifford, K. L. Schmid, and D. A. Atchison, "Effects of eye rotation and contact lens decentration on horizontal peripheral refraction," Ophthalmic Physiol. Opt. **39**(5), 370–377 (2019).

Biomedical Optics EXPRESS

13. A. Mathur, J. Gehrmann, and D. A. Atchison, "Pupil shape as viewed along the horizontal visual field," *J. Vis.* 13, 3(1-8) (2013).
14. V. Ramasubramanian, D. Meyer, P. S. Kollbaum, and A. Bradley, "Experimental model of far temporal field negative dysphotopsia generated in phakic eyes," Invest. Ophthalmol. Visual Sci. **61**(5), 24 (2020).
15. B. H. Altoaimi, P. Kollbaum, D. Meyer, and A. Bradley, "Experimental investigation of accommodation in eyes fit with multifocal contact lenses using a clinical auto-refractor," Ophthalmic Physiol. Opt. **38**(2), 152–163 (2018).
16. L. N. Thibos, X. Hong, A. Bradley, and R. A. Applegate, "Accuracy and precision of objective refraction from wavefront aberrations," J. Vis. **4**(4), 9 (2004).
17. A. Mathur and D. A. Atchison, "Peripheral refraction patterns out to large field angles," Optom. Vis. Sci. **90**(2), 140–147 (2013).
18. D. P. Lopes-Ferreira, H. I. Neves, M. Faria-Ribeiro, A. Queirós, P. R. Fernandes, and J. M. González-Méijome, "Peripheral refraction with eye and head rotation with contact lenses," Cont. Lens. Anterior Eye **38**(2), 104–109 (2015).
19. H. Radhakrishnan and W. N. Charman, "Peripheral refraction measurement: does it matter if one turns the eye or the head?" Ophthalmic Physiol. Opt. **28**(1), 73–82 (2007).
20. A. Mathur, D. A. Atchison, S. Kasthurirangan, N. A. Dietz, S. Luong, S. P. Chin, W. L. Lin, and S. W. Hoo, "The influence of oblique viewing on axial and peripheral refraction for emmetropes and myopes," Ophthalmic Physiol. Opt. **29**(2), 155–161 (2009).
21. L. N. Thibos, W. Wheeler, and D. Horner, "Power vectors: an application of Fourier analysis to the description and statistical analysis of refractive error," Optom. Vis. Sci. **74**(6), 367–375 (1997).
22. A. Mathur and D. A. Atchison, "Effect of orthokeratology on peripheral aberrations of the eye," Optom. Vis. Sci. **86**(5), E476–E484 (2009).
23. D. A. Atchison, D. H. Scott, and W. N. Charman, "Measuring ocular aberrations in the peripheral visual field using Hartmann-Shack aberrometry," J. Opt. Soc. Am. A **24**(9), 2963–2973 (2007).
24. P. Kollbaum, M. Jansen, L. Thibos, and A. Bradley, "Validation of an off-eye contact lens Shack-Hartmann wavefront aberrometer," Optom. Vis. Sci. **85**(9), E817–E828 (2008).
25. A. Mathur, D. A. Atchison, and J. Tabernero, "Effect of age on components of peripheral ocular aberrations," Optom. Vis. Sci. **89**(7), E967–E976 (2012).
26. D. A. Atchison, "Comparison of peripheral refractions determined by different instruments," Optom. Vis. Sci. **80**(9), 655–660 (2003).
27. R. C. Bakaraju, C. Fedtke, K. Ehrmann, and A. Ho, "Comparing the relative peripheral refraction effect of single vision and multifocal contact lenses measured using an autorefractor and an aberrometer: A pilot study," J. Optom. **8**(3), 206–218 (2015).
28. T. O. Salmon, R. W. West, W. Gasser, and T. Kenmore, "Measurement of refractive errors in young myopes using the COAS Shack-Hartmann aberrometer," Optom. Vis. Sci. **80**(1), 6–14 (2003).
29. J. Schwiegerling, J. E. Greivenkamp, and J. M. Miller, "Representation of videokeratoscopic height data with Zernike polynomials," J. Opt. Soc. Am. A **12**(10), 2105–2113 (1995).
30. W. N. Charman, A. Hartwig, A. Mathur, D. H. Scott, and D. A. Atchison, "Specifying peripheral aberrations in visual science," J. Biomed. **17**(2), 025004 (2012).
31. A. B. Watson and J. I. Yellott, "A unified formula for light-adapted pupil size," J Vis. **12**(10), 1–16 (2012).
32. C. E. Campbell, "Determining spherocylindrical correction using four different wavefront error analysis methods: comparison to manifest refraction," J. Refract. Surg. **26**(11), 881–890 (2010).
33. X. Cheng, A. Bradley, and L. N. Thibos, "Predicting subjective judgment of best focus with objective image quality metrics," J. Vis. **4**(8), 310 (2004).
34. P. S. Kollbaum, A. Bradley, and L. N. Thibos, "Comparing the optical properties of soft contact lenses on and off the eye," Optom. Vis. Sci. **90**(9), 924–936 (2013).